The Cryosphere Discuss., 9, 1943–1963, 2015
www.the-cryosphere-discuss.net/9/1943/2015/
doi:10.5194/tcd-9-1943-2015

The Cryosphere Discussions
Open Access

First Sentinel-1 detections of avalanche debris

E. Malnes, M. Eckerstorfer, and H. Vickers

Norut (Northern Research Institute), Dept. Earth Observation, Tromsø Science Park, 9294, Tromsø, Norway

Received: 28 January 2015 – Accepted: 6 March 2015 – Published: 24 March 2015

Correspondence to: E. Malnes (eirik.malnes@norut.no)

Published by Copernicus Publications on behalf of the European Geosciences Union.

Abstract

Snow avalanches are natural hazards, occurring in snow covered mountain terrain worldwide. Present avalanche research and forecasting relies on complete avalanche activity records in a given area over an entire winter season, which cannot be provided with traditional, mainly field based methods. Remote sensing, using weather, and light independent SAR satellites has the potential of filling these data gaps, however, to date their use was limited by high acquisition costs, long repeat cycles, and small ground swath. Sentinel-1A (S1A), on the other hand, operational since October 2014 provides free-of-charge, 20 m spatial resolution, 250 km × 150 km ground swath images every 12 days. In this paper, we present for the first time, that it is possible to detect avalanche debris using S1A images. We successfully apply a change detection method that enhances avalanche debris zones, by comparing repeat pass images before and after the avalanche occurred. Due to the increase in backscatter from avalanche debris, manual detection is possible. With this first proof-of-concept, we show the detection of 489 avalanche debris zones in a S1A image from 6 January 2015, covering the counties Troms and parts of Nordland in Northern Norway. We validate our avalanche detection using very high resolution Radarsat-2 Ultrafine images, as well as extensive field reconnaissance. Our results give us confidence, that S1A detection of avalanches is a critical step towards operational use of SAR avalanche detection in avalanche forecasting.

1 Introduction

Snow avalanches (hereafter called avalanches), cause about 250 fatalities annually, as well as high economic costs due to mitigation measurements and loss of infrastructure (Schweizer, 2008). Avalanche research, is primarily hazard research, focusing on the understanding of avalanche formation in space and time and the resulting consequences. Traditionally, field-testing of snow properties, field reconnaissance of

TCD
9, 1943–1963, 2015

avalanche activity and modelling of both, research the avalanche problem. This approach is handicapped by high-risk exposure and observational bias towards easily accessible areas. Creating a complete avalanche activity record, which is important for forecasting, mitigation and research is thus not possible over an entire winter in any given area.

Remote sensing can potentially fill this data gap by providing safe, unbiased observational data on avalanche activity over fixed areas. To date, ground, air-, and space borne SAR sensors seem to be the most useful tools due to their high to very high resolution, as well as weather and light independency (Bühler et al., 2014). However, their operational use is limited by data availability, high acquisition costs, small ground swaths and long repeat passes.

However, the Sentinel-1A SAR satellite, launched in April 2014, provides free-of-charge, high-resolution SAR data with large ground swath and short repeat time since October 2014. In this short communication, we show for the first time that is possible to detect avalanche debris in Sentinel-1A images. This is an important result for future operational use of SAR data in detecting avalanches over large areas and therefore for creating a complete avalanche record.

1.1 SAR backscatter theory and literature review

The detectable part of an avalanche is its debris, being the snow mass that an avalanche entrains in its slide path. In this paper, we use both avalanche and avalanche debris to describe the same, detectable feature.

A quantitative electromagnetic model of backscatter from avalanche debris is not published. However, Eckerstorfer and Malnes (2014) provided a quantitative interpretation of relative backscatter from dry and wet avalanche debris. Based on the theory of backscatter from undisturbed dry and wet snowpack (Ulaby et al., 1986), increased snow volume, liquid water content, snow density and surface roughness in avalanche debris leads to increased backscatter. They further assume that the backscatter from the air–snow surface interface due to a rough snow avalanche debris surface is the

TCD
9, 1943–1963, 2015

dominant snow parameter that allows for detection of avalanche debris (Eckerstorfer and Malnes, 2014).

The first space-borne SAR detection of avalanches was done by Wiesmann et al. (2001) using ERS1/2 data. A change detection algorithm was applied, utilizing the change in backscatter between two SAR images. Avalanche debris appeared as tongue-shaped features with increased backscatter and sharp backscatter contrast to the surrounding. More recently, Malnes et al. (2013) Eckerstorfer et al. (2014) and Eckerstorfer and Malnes (2014) used both change detection algorithms, as well as single image detection to detect avalanches in Radarsat-2 Ultrafine Mode (RS-2 U) images. Eckerstorfer and Malnes (2014) showed that it is possible to quantify the magnitude of an avalanche cycle in a forecasting region using satellite-borne SAR. However, spatially comprehensive avalanche detection was not achievable, due to the inconsistent availability of RS-2 U data.

2 Dataset and methods

2.1 Meteorology

From the evening of 24 December until 27 December 2014, there was a significant snowfall (at least 50 cm at sea level) onto a thin, weak layer of surface hoar overlaying a hard, consolidated snowpack, and the avalanche risk was increased to 3 (considerable) (varsom.no, 2015). Strong winds from the south between Christmas and New Year transported a large proportion of the new snow predominantly to sheltered northern aspects, leading to snow deposits, which bonded poorly to the snowpack underneath. An intense low-pressure system (also known by the name “Mons”) affected large parts of mid- and northern Norway in the lead-up to New Year. This brought a large rise in temperature to almost 6 ˚ in Tromsø on 30 December, which occurred at the same time with strong winds from the west and heavy rainfall, resulting in a wet and saturated surface snow pack. Consequently, the avalanche risk was upgraded to 4 (high) on New

TCD
9, 1943–1963, 2015

Years Eve (varsom.no, 2015). This period of warm and wet weather conditions lasted until 2 January, which would have led to a short-term destabilisation of the snow pack and triggered the majority of the naturally-released wet slab avalanches in the county.

2.2 SAR image acquisition

Sentinel-1A has a repeat cycle of 12 days. The satellite provides on regular basis 4–5 partial/full coverage over the area we study (counties of Troms and Nordland, Northern Norway) (Fig. 1, green rectangle). The Sentinel-1 IW mode images (Interferometric wide swath) have a spatial resolution of 20 m, and a ground swath of roughly 250 km × 250 km. In addition we also acquired three Radarsat-2 Ultrafine mode images with 3 m spatial resolution and a ground swath of roughly 20 km × 20 km (Fig. 1, red rectangles). Table 1 provides an overview of the SAR images acquired. The reference images are mainly from mid December, when the snowpack was dry and stable, and no avalanche activity was reported (regObs.no, 2015). It is important to choose reference images where the ground conditions are similar to the image with avalanche activity (frozen in our case), the snow is dry, and no avalanche activity occurred.

2.3 SAR image analysis

The Sentinel-1A (S1A) images were downloaded in the standard format ground range detected high-resolution (S1-GRDH) which are focused SAR images, georeferenced to a flat earth ellipsoid with 20 m spatial resolution. All satellite images are acquired in dual-polarization mode (VV and VH). For geocoding, taking into account variable terrain, as well as masking of foreshortening, layover and shadows, we used the GSAR software (Larsen et al., 2005). The result is a radar backscatter image, $\sigma^0(x, y)$ (for VV and VH). We also geocoded the corresponding reference images from the same repeat pass satellite orbit 12 and 24 days earlier at a time before the avalanches had occurred.

Manual avalanche detection in single backscatter images is possible (Eckerstorfer and Malnes, 2014), however, enriched RGB image composites display changes in

TCD
9, 1943–1963, 2015

backscatter in colour, improving manual detection significantly. A RGB composite image (Wiesmann et al., 2001) includes the reference image in the R and B channels, and the current image (with avalanche activity) in the G channel: [R, G, B] = [Ref image, Current image, Ref image]. Each image channel is stretched from its full dynamic range [−35, 10] dB to the range [−25, 5] dB in order to enhance the dominant intensity ranges. The resulting RGB image composite images show wet snow, characterised by a decrease in backscatter (Malnes et al., 2005; Nagler and Rott, 2000) in pink, and avalanche debris, characterised by an increase in backscatter in green. The RGB image composites are stored as geotif-files for manual avalanche detection in a GIS environment.

2.4 Fieldwork validation

In order to validate the SAR interpretations we have collected in-situ data from avalanche debris in the valley Lavangsdalen, easily accessible from the E8 road. Using a handheld GPS, we marked parts of the furthest runout of two wet slab avalanches, that released from the east-facing valley side.

Additionally we took photos of the avalanches, both in the valley Lavangsdalen, and Breivikeidet, confirming that the detected features were really avalanches.

3 Results

3.1 Avalanche debris detection

In a descending path S1A image from 28 December 2014 (not shown), no significant avalanche activity is visible. This drastically changes in the ascending S1A picture from 6 January 2014, which shows a snapshot of avalanche activity from the avalanche cycle of 1–3 January 2015 (Fig. 1). The entire S1A ground swath (250 km × 150 km), covered roughly 23 000 km^2 of land area, spanning over two counties (Troms to the north, Nordland to the south) and nine avalanche forecasting regions (varsom.no, 2015), of

TCD
9, 1943–1963, 2015

which seven are entirely covered (Fig. 1). In this ground swath, 489 avalanches were manually detectable.

These avalanches cluster in areas with steep topography along the fjords. There is a distinct peak of avalanche activity from the town Tromsø towards the southeast (Fig. 1). However, there is also a cluster of avalanche activity in the interior of the county Troms (Fig. 2b). Given the synoptic meteorological condition and the instabilities in the snowpack we expected more avalanche activity in the Lofoten–Vesterålen area than we were able to observe in the S1A image, however the rugged topography, creating significant radar shadow and foreshortening effects, strongly limit the manual detection of avalanche debris (Fig. 2c). Despite the limitation of these radar artefacts, manual detection of avalanche debris is for an experienced observer, relatively straightforward. A strong backscatter contrast, assumed to be of the order of 2–3 dB (Eckerstorfer and Malnes, 2014) between avalanche debris and the surrounding, undisturbed snowpack is used. In most cases, a significant increase in backscatter in avalanche debris and an elongated, tongue shaped signature that extends downslope are indicative (Fig. 2). This change detection method works well in single backscatter images, but the detectability of avalanche debris is considerably increased using RGB image composites.

With a spatial resolution of 20 m in the S1A IW mode, there is a lower limit of detectability. The smallest avalanches detectable were in the order of 80 m × 80 m. It was, however, possible to detect long (> than 150 m) but very thin avalanches with a width of only 3–4 pixels, that released for example in natural terrain features such as gullies. The full extent of the avalanches is not detectable from the SAR images, as it is only the avalanche debris that leads to detectable, increased backscatter due its increased snow depth and surface roughness. Thus we cannot deduct the avalanche starting zone and the avalanche path length from the SAR images.

3.2 Comparison of S1A and RS-2 U images

In Fig. 3 we compare a Radarsat-2 Ultrafine image from 3 January 2015, with a S1A image from 6 January 2015 (similar image that is used in the RGB composite in Figs. 1

TCD
9, 1943–1963, 2015

and 2). In both images, avalanche debris is detectable as light grey features due to increased backscatter. We have used this manual detection method in single RS2-U images successfully to create a record of avalanche activity in the county of Troms in March 2014 (Eckerstorfer and Malnes, 2014). In the RS2-U image, 102 avalanches were detectable within the 20 km × 20 km ground swath (Fig. 3a). The very high spatial resolution of 3 m × 3 m, and the favourable image geometry with only minor areas with radar shadow allow for easy avalanche detection. Therefore, an RS2-U image is to date the reference for satellite-borne SAR avalanche detection. Three days later, 55 out of 102 avalanches were detectable in the lower resolution S1A image (Fig. 3b). The almost 50 % decrease in detectability is due to lower resolution limiting the detectability of small avalanches, and increased radar shadow in the S1A scene, where no avalanches can be detected.

3.3 Fieldwork validation of S1A avalanche debris detection

We drove through the valley Breivikeidet (Fig. 2a), close to Tromsø, 23 January 2015 to take pictures of the detected avalanche debris. A frequently used road leads to Breivikeidet, making field observations easy and efficient.

The valley Lavangsdalen is an avalanche-prone location, where the main road E8 is recurrently endangered from both valley sides (Fig. 3). We collected GPS tracks from two avalanche debris on 8 January 2015. In Fig. 5 we present a multi-sensor, multi-temporal series of SAR images, all from ascending paths, from Lavangsdalen. In the S1A image from 27 December 2014, no avalanche activity is visible. The two features with high backscatter are natural debris flow tracks. Figures 5b, 4c and d, consistently depict avalanche activity that occurred after the avalanche cycle. The collected GPS tracks agree very well with the edge of the avalanche features in all images. This gives us high confidence that we are detecting avalanche debris in the S1A images.

We further took pictures of the avalanche debris for further field validation of the detected avalanche debris, presented in Fig. 6.

TCD
9, 1943–1963, 2015

4 Discussion

Avalanche debris detection in satellite-borne SAR images.

Satellite-borne SAR data has the advantage of weather and light independent image acquisition. This is especially advantageous at northern latitudes, such as the location of our study area, where the Polar night (the sun is below the horizon for two months) largely limits the use of optical data during the winter months.

The clear contrast in backscatter, between avalanche debris with high backscatter and surrounding, undisturbed snowpack with lower backscatter enabled the relatively straightforward visual detection of avalanche debris. The lack of an electromagnetic backscatter model for avalanche debris (disturbed snowpack), as well as the lack of appropriate parameterization of snow parameters in avalanche debris, limits the quantification of the backscatter difference. However, given the comparison between RS2-U and S1A images, as well as the field verification of some detected avalanches, we are confident that we are detecting avalanches. A sharp, clearly delimited increase in backscatter from avalanche debris is due to increased snow depth, snow water equivalent and most importantly increased surface roughness. Thus, we assume that the largest backscatter contribution, which is enhanced under wet snow conditions, stems from surface scattering at the air–snow interface. The total backscatter of wet snow avalanche debris is, however, smaller than that of dry snow avalanche debris (Eckerstorfer and Malnes, 2014; Ulaby et al., 1986).

By creating RGB composite images, using a change detection algorithm of backscatter between two images of the same geometry but acquired at different times, manual avalanche debris detection is further enhanced. The visibility of the backscatter contrast between avalanche debris and surrounding snowpack is enhanced by the stark colour contrast, which enables detection and interpretation also from less experienced observers. This method was until now limited by the availability of reference images with similar geometry, when for example using RS2-U images. There are, however, limitations that become especially apparent in very steep, rugged alpine topography

TCD
9, 1943–1963, 2015

(Fig. 2c). The presence of radar shadows, layover and foreshortening in many areas make avalanche debris detection much more difficult. There are also natural features that have a similar geometry to avalanche debris (e.g. small glaciers, debris from rock fall, debris flows), as well as a strong backscatter contrast to their surroundings. Misinterpreting features as avalanche debris, as well as under detection are problems we cannot quantify yet. We believe however, that more avalanche debris is missed due to radar artefacts than features that have accidentally been interpreted as avalanche debris.

Comparing avalanche debris detection in very high resolution RS2-U and high-resolution S1A images, we find that RS2-U images are technically better suited to the task of detection due to their higher spatial resolution. This allows for detection of small avalanches that are not visible in S1A images. All the large, significant avalanches with run-outs close to a road are, however, clearly detectable in the S1A image. Moreover, acquiring both ascending and descending path S1A images allows for avalanche debris detection at all aspects, at least in the area that is covered by both geometries (i.e. alpine terrain according to the Sentinel-1 high-level operation plan of ESA 2014).

4.1 Operational and research use of S1A avalanche debris detection

In a recent ESA report, Bühler et al. (2014) identified potential users of remote sensing data in avalanche forecasting. Amongst the users were national and regional avalanche warning services that have high willingness-to-pay for auxiliary data provided by remote sensing, due to a large, inaccessible forecasting area and a sparse observational network. One of the main identified data gaps was “avalanche activity”. Requested were hourly temporal resolution, approximately 10 m spatial resolution and very high reliability (Bühler et al., 2014). The report concluded that the only operational product enabling real-time avalanche detection is based on terrestrial radar systems. The report further concluded that satellite-borne radar products do not provide near-real time data on a reliable basis.

TCD
9, 1943–1963, 2015

While S1A products cannot provide near-real time avalanche activity data, they can provide data with a 12 day repeat interval. The main advantage over terrestrial radar systems is the large area covered, which is 250 km × 150 km of ground swath. We believe that as a first step, RGB composite images every 12 days throughout a winter season provide valuable data for an avalanche warning service. The S1A image we present here covers nine forecasting regions, seven of them in entirety. In each forecasting region, two part-time observers and a few low-elevation meteorological stations record avalanche activity, amongst other data. The S1A RGB composite in Fig. 1 provides a valuable visual representation of the magnitude of the avalanche cycle, without marking every detectable avalanche debris. By providing such images over an entire winter season for areas with high reoccurrence of avalanche activity, the forecasted avalanche danger level can be validated. In addition, the magnitude of avalanche cycles due to certain synoptic meteorological conditions can also be analysed. This would then mark an important step towards a much-demanded complete avalanche activity record for a certain area.

Such a complete avalanche activity record is not only of interest for avalanche warning services, but also critical in avalanche research. Such complete datasets are of great importance for statistical avalanche forecasting (Buser, 1983; Eckerstorfer and Christiansen, 2011; Föhn et al., 1977; Hendrikx et al., 2014), to return-period calculations (Eckert et al., 2010), identification of avalanche hazard on infrastructure (Hendrikx and Owens, 2008; Margreth et al., 2003), and increasingly climate change related studies (Fitzharris and Schaerer, 1980; Marty and Meister, 2012).

For these applications however, all avalanche debris needs to be detected and recorded in a geospatial database. However, the accumulation of large datasets may become problematic for the analysis and storage of data. Manual detection of avalanche debris in a handful of S1A scenes every 12 days is labour intensive and time consuming. Thus, an automatic avalanche debris detection algorithm is needed. Such a detection algorithm could utilize the backscatter contrast, as well as the typical morphological features of avalanche debris. By further identifying and neglecting ter-

TCD
9, 1943–1963, 2015

rain where avalanche debris is unlikely to occur (based on slope angle, dense forest cover), the algorithm would have less pixels to search for, which would reduce computational problems.

5 Conclusion

In this study, we show for the first time, that Sentinel-1A images in interferometric wide swath mode (IW) (20 m × 20 m spatial resolution) can be used to manually detect avalanche debris. The minimum extent of detected avalanche debris was roughly 80 m × 80 m. In the 250 km × 150 km large ground swath of the S1A image, we detected 489 avalanches, from a wet snow avalanche cycle that occurred around 1 January 2015. To detect avalanches, we utilized the increase in backscatter from avalanche debris with increased snow depth, SWE, and most importantly, surface roughness. Tongue-shaped features, with a sharp backscatter contrast to the surrounding, undisturbed snowpack, allow for straight-forward manual detection. This change detection approach is further enhanced by generating RGB image composite, with the reference image in the R and B channels, and the current image in the G channel. Avalanche debris appears in bright green colours. To validate the avalanche detections, we did field reconnaissance trips to some accessible avalanches around Tromsø, as well as compared the S1A results with detection in RS-2 U images, which have a spatial resolution of 3 m × 3 m.

We are confident that avalanche detection using S1A images as a first critical step towards operational use of SAR data in avalanche forecasting. This is mainly due to the free-of-cost availability of at least two images per 12 day repeat cycle, the weather and light independency, and the large ground swath. Thus, significant avalanche activity can be monitored throughout a winter in a large forecasting region. However, manual detection is time consuming, thus automatic avalanche detecting algorithms need to be improved, in order to automate the entire processing chain.

TCD
9, 1943–1963, 2015

Acknowledgements. This research is financed by RDA Troms (competence centers in and for northern environments). Radarsat-2 images were acquired under the Norwegian RS-2 agreement. Sentinel-1A data was acquired from the Sentinel-1 Scientific Data Hub.

References

Bühler, Y., Bieler, C., Pielmeier, C., Frauenfelder, R., Jaedicke, C., Bippus, G., Wiesmann, A., and Caduff, R.: Improved Alpine Avalanche Forecast Service, Final Report, WSL Institute for Snow and Avalanche Research SLF, Davos, Switzerland, 22 pp., 2014.

Buser, O.: Avalanche forecast with the method of nearest neighbours: an interactive approach, Cold Reg. Sci. Technol., 8, 155–163, 1983.

Eckerstorfer, M. and Christiansen, H. H.: Relating meteorological variables to the natural slab avalanche regime in High Arctic Svalbard, Cold Reg. Sci. Technol., 69, 184–193, 2011.

Eckerstorfer, M. and Malnes, E.: Multi-sensor and multi-temporal avalanche debris detection using SAR and optiacl remote sensing data, Cold Reg. Sci. Technol., 19, submitted, 2014.

Eckerstorfer, M., Malnes, E., Frauenfelder, R., Domaas, U., and Brattlien, K.: Avalanche debris detection using satellite-borne radar and optical remote sensing, in: Proceedings of the International Snow Science Workshop 2014, Banff, Canada, 29 September–3 October, 122–128, 2014.

Eckert, N., Coleou, C., Castebrunet, H., Dechatres, M., Giraud, G., and Gaume, J.: Cross-comparison of meteorological and avalanche data for characterising avalanche cycles: the example of December 2008 in the eastern part of the French Alps, Cold Reg. Sci. Technol., 64, doi:10.1016/j.coldregions.2010.08.009, 2010.

Fitzharris, B. B. and Schaerer, P.: Frequency of major avalanche winters, J. Glaciol., 26, 43–48, 1980.

Föhn, P., Good, W., Bois, P., and Obled, C.: Evaluation and comparison of statistical and conventional methods of forecasting avalanche hazars, J. Glaciol., 19, 375–387, 1977.

Hendrikx, J. and Owens, I.: Modified avalanche risk equations to account for waiting traffic on avalanche prone roads, Cold Reg. Sci. Technol., 51, 214–218, 2008.

Hendrikx, J., Murphy, M., and Onslow, T.: Classification trees as a tool for operational avalanche forecasting on the Seward Highway, Alaska, Cold Reg. Sci. Technol., 97, 113–120, 2014.

TCD
9, 1943–1963, 2015

Larsen, Y., Engen, G., Lauknes, T. R., Malnes, E., and Høgda, K. A.: A generic differential interferometric SAR processing system, with applications to land subsidence and snow-water equivalent retrieval, Fringe ATSR Workshop 2005, Frascati, Italy, 28 November–2 December, 6, 2005.

Malnes, E., Storvold, R., Lauknes, I., Solbø, S. A., Solberg, R., Amlien, J., and Koren, H.: Multi-sensor monitoring of snow parameters in Nordic mountainous areas, in: Geoscience and Remote Sensing Symposium (IGARSS 05), Seoul, South Korea, 25–29 July 2005, 1951–1954, 2005.

Malnes, E., Eckerstorfer, M., Larsen, Y., Frauenfelder, R., Jonsson, A., Jaedicke, C., and Solbø, S. A.: Remote sensing of avalanches in northern Norway using Synthetic Aperture Radar, in: Proceedings of the International Snow Science Workshop 2013, Grenoble – Chamonix, Mont Blanc, France, 9–13 October, 955–959, 2013.

Margreth, S., Stoffel, L., and Wilhelm, C.: Winter opening of high alpine pass roads – analysis and case studies from the Swiss Alps, Cold Reg. Sci. Technol., 37, 467–482, 2003.

Marty, C. and Meister, R.: Long-term snow and weather observations at Weissfluhjoch and its relation to other high-altitude observatories in the Alps, Theor. Appl. Climatol., 110, 573–583, doi:10.1007/s00704-012-0584-3 2012. 2012.

Nagler, T. and Rott, H.: Retrieval of wet snow by means of multitemporal SAR data, IEEE T. Geosci. Remote, 38, 754–765, 2000.

Schweizer, J.: Snow avalanche formation and dynamics, Cold Reg. Sci. Technol., 54, 153–154, 2008.

Ulaby, F. T., Moore, R. K., and Fung, A. K.: Microwave Remote Sensing: Active and Passive; From Theory to Applications, Artech House, Norwood, 1986.

Wiesmann, A., Wegmueller, U., Honikel, M., Strozzi, T., and Werner, C. L.: Potential and Methodology of Satellite Based SAR for Hazard Mapping, IGARSS 2001, Sydney, Australia, 9–13 July 2001.

TCD
9, 1943–1963, 2015

Table 1. Overview of acquired SAR images, both S1A and RS2 images.

Date	Mode	Date	Path	Ref. image
S1A	IW	27.12.2014	ACS	15.12.2014
S1A	IW	28.12.2014	DES	16.12.2014
RS2	U73	01.01.2015	ASC	No reference image
RS2	U13	02.01.2015	DES	No reference image
RS2	U24	03.01.2015	ASC	No reference image
S1A	IW	06.01.2015	ASC	13.12.2014
S1A	IW	08.01.2015	ASC	13.12.2014

TCD
9, 1943–1963, 2015

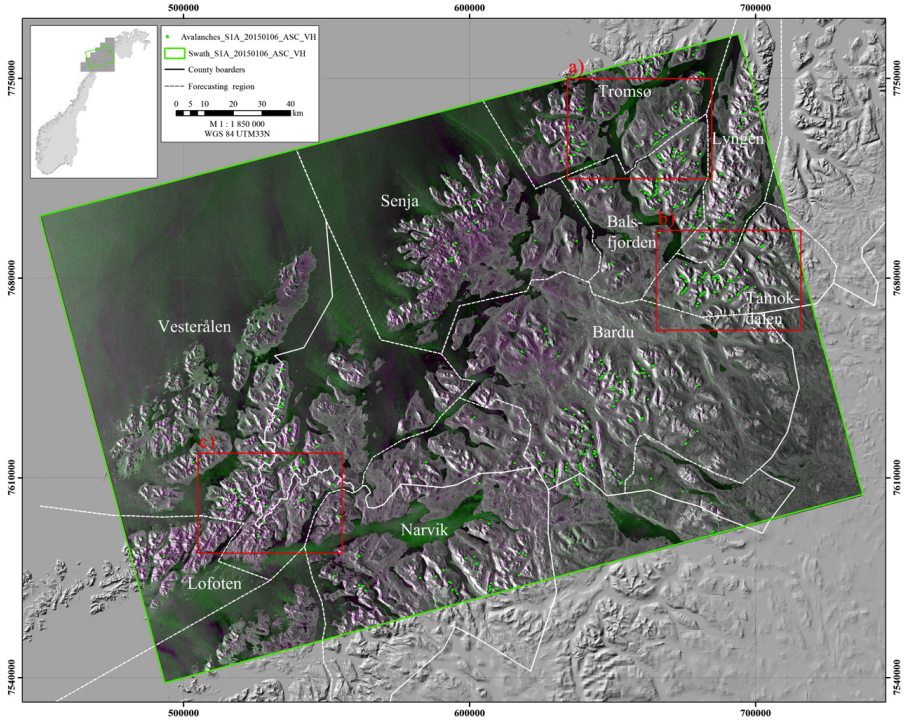

Figure 1. S1A RGB image composite, where two S1A images with similar ascending path are merged. The reference image is from 13 December 2014, visualized in the green channel, the image from 6 January 2015 is visualized in the red and blue channel. Avalanche debris appears as green, tongues-shaped features; the furthest runout location is marked with a green point. The purple colour indicates a change in physical snow parameters, most likely a change from dry to wet snow. The three red rectangles depict areas of interest, shown in Fig. 2.

TCD
9, 1943–1963, 2015

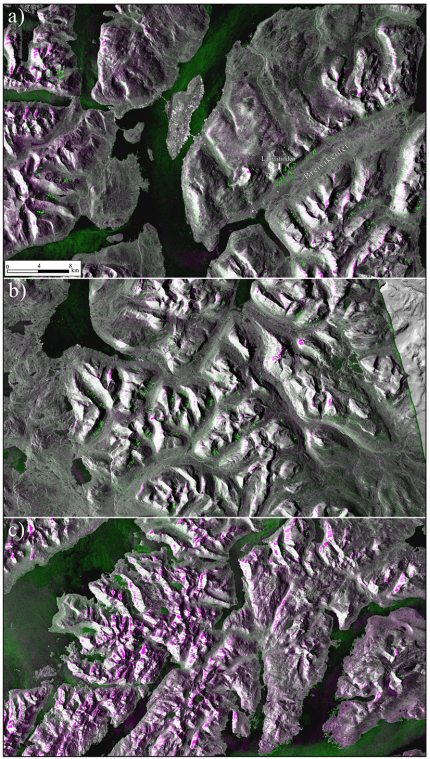

Figure 2. Three areas of interest from the S1A RGB image composite in Fig. 1 (red rectangles). Avalanche debris appears as green, tongues-shaped features; the furthest runout location is marked with a green point. The purple colour indicates a change in physical snow parameters, most likely a change from dry to wet snow. The numbered avalanches in Breivikeidet valley in **(a)** correspond to field validated avalanches.

TCD
9, 1943–1963, 2015

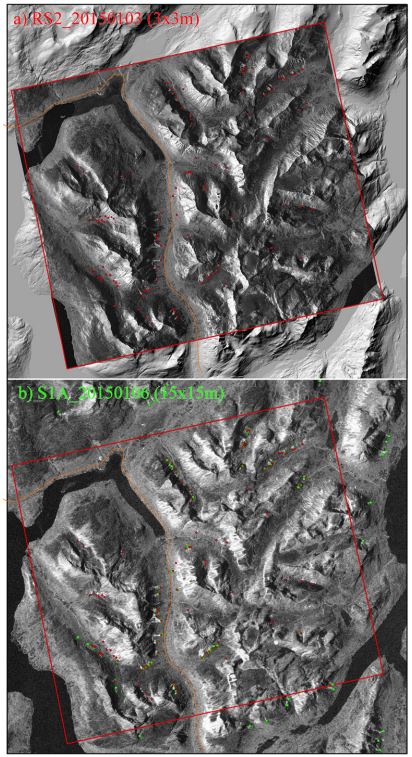

Figure 3. Comparison between a Radarsat-2 Ultrafine (RS2-U) image from 3 January 2015 **(a)** and a part of a Sentinel-1A (S1A) image from 6 January 2015 **(b)**. Coloured points (RS2-U detection in red, S1A detection in green) depict the furthest runout of detected avalanches. The orange line is the main road E8, running through the valley.

TCD
9, 1943–1963, 2015

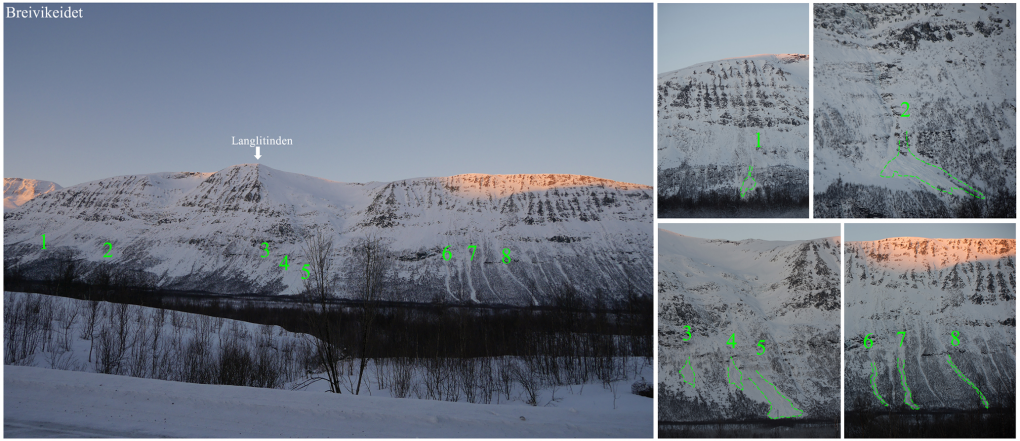

Figure 4. Fieldwork validation of detected avalanche debris in the valley Breivikeidet, 23 January 2015. Avalanche debris was still clearly visible then, as the period since New Year was dry and cold. The numbers correspond to the detected avalanche debris in Fig. 2a.

TCD
9, 1943–1963, 2015

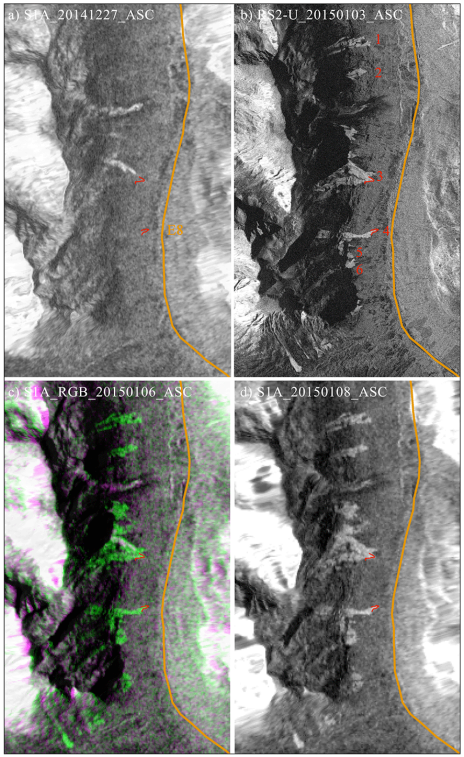

Figure 5. Multi-sensor and multi-temporal series of SAR images from Lavangsdalen valley, containing ascending path S1A and RS2-U images. The road E8 through Lavangsdalen valley is in orange. The collected GPS tracks of two avalanche debris are visualized with red lines.

TCD
9, 1943–1963, 2015

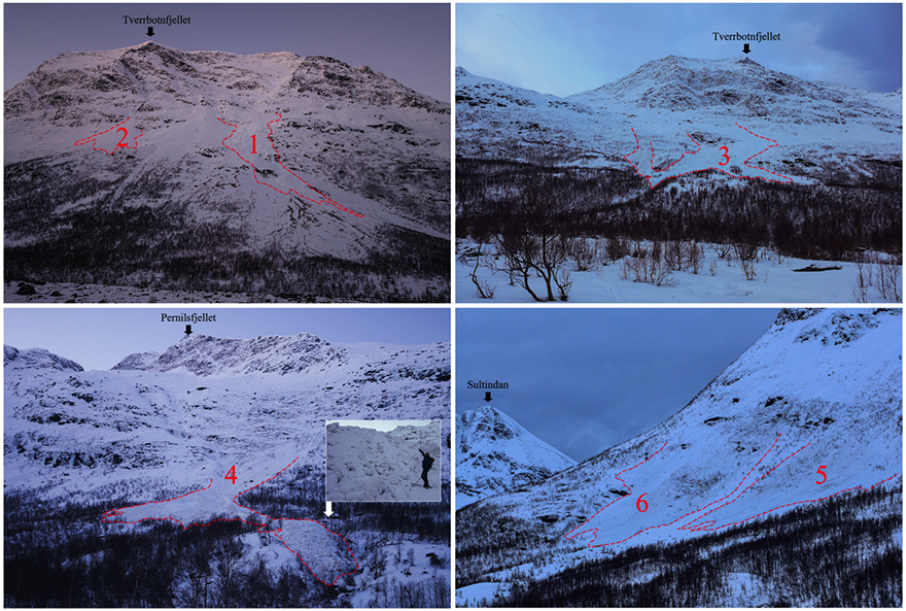

Figure 6. Fieldwork validation of detected avalanche debris in the valley Lavangsdalen, 8 January 2015. Avalanche debris was still clearly visible then, as the period since New Year was dry and cold. The numbers correspond to the detected avalanche debris in Fig. 5b.

TCD
9, 1943–1963, 2015